Published in final edited form as:
Water Res. 2012 September 15; 46(14): 4521–4531. doi:10.1016/j.watres.2012.05.036.

Transport Behavior of Functionalized Multi-Wall Carbon Nanotubes in Water-Saturated Quartz Sand as a Function of Tube Length

Yonggang Wang[a], **Jae-Hong Kim**[b], **Jong-Beom Baek**[c], **Gary W. Miller**[d], and **Kurt D. Pennell**[a,*]

[a]Department of Civil and Environmental Engineering, Tufts University, 200 College Ave, Medford, MA 02155

[b]School of Civil and Environmental Engineering, Georgia Institute of Technology, 200 Bobby Dodd Way, Atlanta, GA 30332

[c]Interdisciplinary School of Green Energy/Institute of Advanced Materials & Devices, Ulsan National Institute of Science and Technology, Ulsan, 689-798 South Korea

[d]Department of Environmental Health, Rollins School of Public Health, Emory University, 1518 Clifton Road, Atlanta, GA 30322

Abstract

A series of one-dimensional column experiments was conducted to examine the effects of tube length on the transport and deposition of 4-ethoxybenzoic acid functionalized multi-wall carbon nanotubes (MWCNTs) in water-saturated porous media. Aqueous MWCNTs suspensions were prepared to yield three distributions of tube lengths; 0.02–1.3 μm (short), 0.2–7.5 μm (medium), and 0.2–21.4 μm (long). Results of the column studies showed that MWCNT retention increased with increasing tube length. Nevertheless, more than 76% of the MWCNT mass delivered to the columns was detected in effluent samples under all experimental conditions, indicating that the functionalized MWCNTs were readily transported through 40–50 mesh Ottawa sand. Examination of MWCNT length distributions in the effluent samples revealed that nanotubes with lengths greater than 8 μm were preferentially deposited. In addition, measured retention profiles exhibited the greatest MWCNT deposition near the column inlet, which was most pronounced for the long MWCNTs, and decreased sharply with travel distance. Scanning electron microscope (SEM) images showed that MWCNTs were deposited on sand surfaces over the entire column length, while larger MWCNT bundles were retained at grain intersections and near the column inlet. A mathematical model based on clean bed filtration theory (CBFT) was unable to accurately simulate the measured retention profile data, even after varying the weighting function and incorporating a nonuniform attachment rate coefficient expression. Modification of the mathematical model to account for physical straining greatly improved predictions of MWCNT retention, yielding straining rate coefficients that were four orders-of-magnitude greater than

*Corresponding author: Kurt D. Pennell, Ph.D., P.E. Department of Civil and Environmental Engineering Tufts University 200 College Avenue Medford, MA 02155 Tel: 617-627-3099 fax: 617-627-3994 kurt.pennell@tufts.edu.

Appendix. Supplementary Information Supplementary information, including descriptions of CBFT model refinements to account for rod-shaped particles and a distributed attachment rate coefficient, a summary of model paremeter output, DLS size distributions, and additional comparisons between model predictions and measured data, can found in the online version of this article at doi:xxxx

corresponding attachment rate coefficients. Taken in concert, these experimental and modeling results demonstrate the potential importance of, and need to consider, particle straining and tube length distribution when describing MWCNT transport in water-saturated porous media.

Keywords

multi-wall carbon nanotubes; MWCNTs; tube length; transport; retention; attachment; straining

1. Introduction

Carbon nanotubes (CNTs) are tubular carbon macro-molecules with diameters of a few to tens of nanometers and lengths of micrometers up to a few centimeters (Wang et al., 2009). Due to their unique physical and chemical properties, CNTs have been used in various applications, including solar cells, sensors, and high strength composites (Kong et al., 2000; Gannon et al., 2007; Li et al., 2007). Although CNTs are hydrophobic and exhibit large aspect ratio, stable aqueous suspensions of multi-wall carbon nanotube (MWCNT) can be readily prepared when their surface is coated with surfactant, polymer, or natural organic matter (Hyung et al., 2007), or is chemically functionalized (Sun et al., 2002). The stability of these functionalized CNTs will facilitate their release and persistence in aquatic environments, and may enhance their potential toxicity. CNTs suspended in water or culture media were found to exhibit cytotoxicity (Hussain et al., 2009), as evidenced by growth inhibition of human HEK293 kidney cells (Cui et al., 2005) and morphological changes in A549 lung cells (Davoren et al., 2007). The potential aqueous stability and health impacts of functionalized CNTs necessitate a more comprehensive understanding of their fate and transport in the porous media, which is critical for the design of effective removal strategies for drinking water treatment and protection of groundwater resources.

To date, a limited number of experimental studies have been performed to investigate single-wall carbon nanotube (SWCNT) and MWCNT transport and deposition in porous media (Lecoanet et al., 2004; Lecoanet and Wiesner, 2004; Jaisi et al., 2008; Jaisi and Elimelech, 2009; Wang et al., 2008a; Lui et al., 2009). In these studies, ultrasonication was often applied to overcome the strong lateral van der Waals interactions between tubes, and the surface was either stabilized with surfactant (Lecoanet et al., 2004; Lecoanet and Wiesner, 2004) or humic acid (Wang et al., 2008a), or functionalized with hydroxyl or carboxyl groups via strong acid treatment (Jaisi et al., 2008; Jaisi and Elimelech, 2009; Lui et al., 2009). Additionally, relatively high nanotube input concentrations (e.g., 100 mg/L) were employed to allow for quantification based on ultraviolet (UV) light absorbance. At low ionic strength (0.01 mM), surfactant- or humic acid (HA)-stabilized SWCNTs exhibited relatively high mobility in columns packed with glass beads or clean sands compared to other nanoparticles and natural colloids (Lecoanet et al., 2004; Wang et al., 2008a). Transport experiments conducted with carboxyl (-COOH) functionalized SWCNTs suggest that physical straining played a role in nanotube retention at low ionic strength (< 0.03 mM), which was most pronounced in aggregated soil (Jaisi et al.; 2008; Jaisi and Elimelech, 2009). Several studies reported effective hydrodynamic radii based on dynamic light scattering (DLS) measurements, which were typically one order-of-magnitude smaller than the lengths observed by transmission electron microscopy (TEM) (e.g., Lecoanet et al., 2004). However, none of these studies directly evaluated the effects of tube length and aspect ratio on the transport and retention of CNTs.

Although mathematical modeling of carbon nanotube transport and deposition in porous media is limited, several researchers employed clean-bed filtration theory (CBFT) to interpret SWCNT and MWCNT experimental observations (Lecoanet et al., 2004; Jaisi et

al., 2008; Jaisi and Elimelech, 2009; Wang et al., 2008a). Based on "steady-state" effluent concentration data, CBFT was utilized to obtain attachment rate coefficients (k_{att}) and theoretical column (bed) lengths necessary to achieve for 3-log (99.9%) reduction (L_{max}). For example, L_{max} values obtained for HA-stabilized MWCNTs in clean sand increased from 0.1 to 2.8 m when the ionic strength was decreased from 10 to 0.01 mM (Wang et al., 2008a). More recently, a modified CBFT model that incorporates time-dependent site-blocking kinetics and a nanotube shape factor was employed to fit MWCNT effluent breakthrough curves (BTCs) obtained using a water-saturated quartz sand (d_{50}=476 um, 30–40 mesh) at pore-water velocities ranging from 0.42 to 43 m/d (Lui et al., 2009). Although this modified model yielded reasonable predictions of MWCNT effluent data, the potential contribution of physical straining as a retention mechanism was not considered. This omission could be significant because recent studies of carboxyl-(COOH) functionalized SWCNT transport in a quartz sand and an aggregated soil suggest that physical straining plays a key role in CNT retention, particularly at low ionic strength (Jaisi et al., 2008; Jaisi and Elimelech, 2009). However, CNT retention profiles (i.e., solid-phase concentrations as a function of distance from the column inlet) were not measured in any of the CNT transport studies reported to date, precluding direct assessment of CBFT applicability to modeling CNT transport in porous media.

The objectives of this study were two-fold; first to investigate the effects of tube length on the transport and retention of MWCNTs in water-saturated quartz sand, and second to directly assess the role of physical straining based on measured MWCNT retention profiles. A novel chemical modification method, which disperses CNTs in water with minimal structural damage, was employed to prepare aqueous suspensions of MWCNTs with three tube lengths: 0.02–1.3, 0.2–7.5, and 0.2–21.4 μm. A series of one-dimensional (1-D) transport experiments were then performed in water-saturated quartz sand to obtain MWCNT effluent BTCs and solid-phase retention profiles. The resulting experimental data were simulated using mathematical models based on traditional CBFT, corrected for rod-shaped particles, or modified to incorporate a physical straining term. Scanning electron microscope (SEM) images were collected to provide direct observations of MWCNT retention within the porous medium.

2. Materials and methods

2.1. Preparation of stable MWCNT suspensions

MWCNTs with three different length classes, 0.5–2 μm (short), 10–30 μm (medium), and 100 μm (long), were purchased from Cheap Tubes Inc. (Brattleboro, VT). According to the manufacturer, the purity of the MWCNTs was greater than 95% (wt), consisting of 99.8% carbon, negligible metals, and an ash content of less than 1.5%. The manufacturer-reported outside diameter of the short and medium MWCNTs was 10–20 nm, while that of the long MWCNTs was 8–15 nm. Reagent grade polyphosphoric acid (PPA), phosphorus pentoxide (P_2O_5), and 4-ethoxybenzoic acid (4-EBAc) were obtained from Sigma-Aldrich Inc. (St. Louis, MO).

Aqueous MWCNT suspensions were prepared following previously described protocols (Lee et al., 2008). Briefly, MWCNTs, 4-EBAc, PPA, and P_2O_5 were mixed in a 250 mL resin flask (ACE Glass Inc., Vineland, NJ) at a weight ratio of 1:1:40:10 under a N_2 gas atmosphere. The reaction temperature was sequentially increased from 80 °C for 1 h, 100 °C for 1 h, and 130 °C for 72 h. Approximately 950 mL of degassed de-ionized (DI) water was then added to the mixture to obtain a stock suspension with a final MWCNT concentration of approximately 1 g/L. The stock suspension was stored in the dark at room temperature, and all the transport experiments were completed within one week following preparation of each stock. To prepare influent suspensions for the column experiments, a predetermined

amount of stock suspension was mixed with degassed DI water and adjusted to pH 5 with 0.1 M NaOH. Due to the presence of residual phosphate ions in the stock, the ionic strength of the MWCNT input suspension was calculated based upon concentrations of $H_2PO_4^-$, HPO_4^{2-}, HPO_4^{3-}, and Na^+ and further adjusted, if necessary, using sodium chloride.

2.2. Characterization of functionalized MWCNTs

The mean hydrodynamic diameter and electrophoretic mobility (EM) of MWCNTs were determined by DLS and laser Doppler velocimetry, respectively, using a Zetasizer NanoZS analyzer (Malvern Instruments, Southborough, MA) equipped with a red laser that was operated at a wavelength of 633 nm and in back scattering mode at an angle of 173°. All measurements were performed in triplicate and at room temperature (23 ± 1 °C). The NanoZS analyzer was calibrated using a mono-disperse suspension of polystyrene spheres (Nanosphere Size Standards, Duke Scientific, Palo Alto, CA) with a mean diameter of 97 ± 3 nm and a zeta potential transfer standard (Malvern Instruments Ltd.) with a mean zeta potential of −68 ± 6.8 mV.

MWCNTs in column influent suspensions and selected effluent samples were further characterized using a JEM-2100 LaB6 TEM (JEOL Ltd., Tokyo, Japan) operated at 200 kV. To prepare a TEM specimen, a drop of MWCNT suspension was placed on a 400-mesh carbon-coated copper grid (Electron Microscopy Sciences, Hatfield, PA), allowed to equilibrate for two minutes, and the excess liquid was gently blotted using a Kimwipe® tissue prior to being air-dried overnight. This specimen preparation method was chosen to minimize the crystallization of background salts. The image processing software ImageJ version 1.42q (Rasband, 2011) was utilized to quantify nanotube diameter and length. At least 10 images were collected for each specimen at random grid locations and the length of all observed nanotubes on each image was measured, which resulted in no less than 200 measurements for each specimen. The spectroscopic properties of 4-EBAc functionalized MWCNTs prepared using the same protocol have been previously reported (Lee et al., 2008).

Images of MWCNTs retained near the column inlet and outlet were obtained using a scanning electron microscope (SEM). The SEM samples were prepared by attaching an aluminum mount stub (Electron Microscopy Sciences) covered with a piece of conductive carbon tape (Electron Microscopy Sciences) onto sands collected from the column immediately after a medium-long MWCNT transport experiment was completed. The samples were then air-dried overnight and analyzed using a Zeiss Ultra Plus field emission SEM (Carl Zeiss Microscopy, LLC, Peabody, MA) with charge compensation operated at 3 kV.

2.3. Column transport and retention experiments

The column apparatus consisted of a high-performance liquid chromatography (HPLC) pump (ChromTech, Inc., Apple Valley, MN) to deliver background electrolyte and non-reactive tracer solutions, a syringe pump (Harvard Apparatus, Holliston, MA) to introduce MWCNT suspensions, a borosilicate glass column (Kontes, Vineland, NJ) with an inside diameter of 2.5 cm and length of 10 cm, and a fraction collector (Spectrum Chromatography, Houston, TX) to collect effluent samples. The column was equipped with two endplates fitted with two 60-mesh stainless steel screens (Gerard Daniel Worldwide, Inc., Hanover, PA) and was packed with air-dried 40–50 mesh (d_{50} = 0.36 mm) Ottawa sand (U.S. Silica, Berkeley Springs, WV) in 1-cm increments. Prior to use, the sand was treated to remove residual organic matter and natural colloids following an existing protocol (Wang et al., 2008b). The packed column was then purged with CO_2 gas for at least 15 min to facilitate the rapid dissolution of entrapped gas during the water imbibition process. At least

10 pore volumes (PVs) of degassed background electrolyte (6 or 75 mM NaCl) solution were introduced in a down-flow mode. In the first set of transport experiments, a pulse (ca. 5 PVs) of MWCNT suspension (10 mg/L) with an ionic strength of 6 mM was delivered to the column at a flow rate of 1.0 mL/min, which corresponded to a pore-water velocity of ca. 7.6 m/d, followed by the introduction of 3 PVs of MWCNT-free solution at the same flow rate. Column effluent samples were collected continuously in 15-mL sterile plastic centrifuge tubes (VWR International, West Chester, PA) using a fraction collector. At the conclusion of each transport experiment, eight equal-length sections were removed from the column using a spatula. De-ionized water (10 mL) was added to each solid sample and ultrasonication (Fisher Scientific, Fair Lawn, NJ) was applied for 1 min to extract retained MWCNTs. A sand blank sample (free of MWCNT) was prepared in the same manner to account for any background contributions. A second set of transport experiments with both high input concentration (90 mg/L) and ionic strength (75 mM) was conducted at the same flow rate and pulse injection procedure to allow for comparisons to prior studies.

Concentrations of MWCNTs in aqueous samples were determined using a UV-Vis spectrophotometer (Shimadzu Scientific Instruments, Columbia, MD). The absorbance response at a wavelength of 800 nm, which corresponded to light scattering by suspended MWCNTs, was used for quantification based on a five-point calibration curve prepared by serial dilution of a MWCNT stock suspension of known concentration in plastic tubes. While a 10-mm path length quartz cuvette was used for experiments with a MWCNT input concentration of 90 mg/L, a quartz cuvette with 50-mm optical path length was required for effluent samples collected in experiments with the input concentration of 10 mg/L. Overall mass balance of MWCNTs measured in the column effluent and retained by the solid phase ranged from 90 to 102% of the applied mass.

In selected column studies, a non-reactive tracer test was conducted to assess water flow and hydrodynamic dispersion prior to MWCNT injection. Five PVs of sodium bromide solution at the same ionic strength and pH as the background solution were injected into the column at the same flow rate (1.0 mL/min), followed by three PVs of background solution. Effluent samples were collected continuously and bromide concentrations were measured using an ion selective bromide probe (Cole-Parmer Instrument Co., Vernon Hills, IL) connected to an Accumet Model 50 pH meter (Fisher Scientific).

2.4. Mathematical modeling

Assuming conditions of homogeneity, laminar flow, and negligible decay, the transport of MWCNTs in a one-dimensional (1-D) water-saturated porous medium can be described by advection, dispersion, and deposition processes as (Wang et al., 2008b):

$$\frac{\partial C}{\partial t} = D_H \frac{\partial^2 C}{\partial \chi^2} - v_p \frac{\partial C}{\partial \chi} - \frac{\rho_b}{\theta_w} \frac{\partial S}{\partial t} \quad (1)$$

where C is the MWCNT concentration in the aqueous phase, S is the MWCNT concentration associated with the solid phase, D_H is the hydrodynamic dispersion coefficient, x is the travel distance, t is time, θ_w is the volumetric water content, ρ_b is the solid phase bulk density, and v_p is the pore-water velocity. To provide baseline CBFT simulations and to allow for comparisons with prior studies (e.g., Lecoanet et al., 2004), MWCNT effluent and retention profile data were initially fit to a model that described nanoparticle deposition using first-order attachment kinetics:

$$\frac{\rho_b}{\theta_w} \frac{\partial S}{\partial t} = k_{att} C \quad (2)$$

where the attachment rate coefficient, k_{att}, is expressed as:

$$k_{att}=\frac{3\,(1-\theta_w)\,v_p}{2d_c}\alpha\eta_0 \tag{3}$$

Here, the attachment efficiency, α, represents the fraction of MWCNTs that remain attached after collision, the single collector efficiency, η_0, represents the frequency of MWCNT collision to solid surface, modified to account for the large nanotube shape factor (Lui et al., 2009;see Supplementary material), and d_c denotes the mean grain size. In the second modeling approach, the deposition process is described by a combination of first-order attachment and physical straining:

$$\frac{\rho_b}{\theta_w}\frac{\partial S}{\partial t}=k_{att}C+k_{str}\psi C \tag{4}$$

where k_{str} is the straining rate coefficient and ψ is the depth-dependent blocking coefficient, expressed as (Bradford et al., 2003):

$$\psi=\left(\frac{d_c+\chi}{d_c}\right)^{-\beta} \tag{5}$$

where β is an empirical factor with a value of 0.8, which represents the best fit to present transport and retention data. Eqs. (1)–(5) were solved using the Hydrus-1D model, version 4.14 (Šimůnek et al., 2008) with k_{att} and k_{str} as fitting parameters. Non-reactive tracer BTCs were fit to the dimensionless form of the 1-D advective-dispersive-reactive (ADR) transport Eq. (1) using CXTFIT ver. 2.0 (Toride et al., 1999) to independently obtain D_H and assess flow conditions.

3. Results

3.1. Properties of functionalized MWCNT suspensions

TEM images of short, medium, and long classes of functionalized MWCNTs obtained from the column influent suspensions are shown in Figs. S1A, S1B, and S1C, respectively. These images indicate that individual (i.e., non-bundled) MWCNTs exist in all of the suspensions. Analysis of the TEM images revealed that the diameters of short, medium, and long MWCNTs ranged from 10–30 nm, 10–40 nm, and 30–70 nm, respectively. Tube length distributions obtained for MWCNTs in the column influent suspensions are presented in Fig. 1 (denoted as 0 PV). The TEM-determined length of MWCNTs in the short, medium and long suspensions ranged from 0.02 to 1.3μm, 0.2 to 7.5 μm, and from 0.2 to 21.4 μm, with a mean length ± standard deviation of 0.15 ± 0.15 μm (4.2), 1.14 ± 1.04 μm (3.2), and 1.69 ± 1.91 μm (5.9), respectively.

Despite the large aspect ratio of nanotubes, DLS has been widely used to measure the hydrodynamic diameter and size distribution of CNTs in aqueous suspension (e.g., Lecoanet et al., 2004; Jaisi and Elimelech, 2009). In the present study, MWCNT size information obtained by DLS was reported in two forms; the mean hydrodynamic diameter obtained by fitting the correlation function to a single exponential function, and the particle size distribution, based on fitting the correlation function to multiple exponential functions (Jiang et al., 2009). The mean hydrodynamic diameter of the short, medium, and long MWCNTs ranged from 211–334 nm, 313–408 nm, and 600–795 nm, respectively (Table S1).

All of the dispersed MWCNTs exhibited a negative charge, with electrophoretic mobility (EM) values ranging from −2.6 to −3.8 μm·cm/V·s (Table 1). For the influent MWCNT

concentration of 10 mg/L, the measured EM values increased incrementally from −3.0 to −3.8 μm·cm/V·s with increasing mean tube length., Similarly, for 90 mg/L influent concentration EM values increased from −2.6 to −3.2 μm·cm/V·s with increasing tube length. Based on the Smoluchowski model (Hiemenez and Rajagopalan, 1997), the calculated zeta potential of the medium-size fraction MWCNTs ranged from −38.0 to −43.6 mV, consistent with values reported by (Wang et al., 2008a). Since no oxidizing agent (e.g., nitric acid) or ultrasonication was used during functionalization with 4-EBAc, EM and zeta potential values were less negative compared to MWCNTs functionalized with hydroxyl or carboxyl groups (Liu et al., 2009).

3.2. Transport and retention of MWCNTs

Relative effluent MWCNT concentrations (C/C_0, where C is measured effluent concentration and C_0 is the influent concentration) were plotted against the number of dimensionless pore volumes (PV = $v_p \times t/L$) of influent solution introduced into the column. The resulting effluent BTCs obtained in 40–50 mesh Ottawa sand for three MWCNT size fractions at influent concentrations of 10 and 90 mg/L are shown in Figs. 2A and 2C, respectively. Regardless of tube length and input concentration, MWCNTs were detected in the column effluent after approximately one PV, coinciding with breakthrough of the non-reactive tracer. In general, the relative MWCNT concentrations rapidly increased to a plateau, and then decreased sharply after introducing the MWCNT-free background, and quickly reached non-detectable levels. Mobility of MWCNTs was strongly dependent upon tube length, with the effluent plateau levels decreasing from relative concentration (C/C_0) values of 0.97 to 0.71 as the measured tube length increased from short (0.2–1.3 μm) to long (0.2–21.4 μm). Nevertheless, functionalized MWCNTs were readily transported through water-saturated 40–50 mesh Ottawa sand (d_{50} = 0.36 mm), with greater than 76% of the introduced mass appearing in the column effluent even for the longest tube lengths (0.2 to 21.4 μm).

At the conclusion of each transport experiment, the column was sectioned into 1-cm increments and attached CNTs were extracted to obtain MWCNT retention profiles, plotted as the solid-phase concentration versus the distance from the column inlet. Measured retention profiles for input concentrations of 10 and 90 mg/L are presented in Figs. 2B and 2D, respectively. These data provide quantitative information on the spatial distribution of deposited MWCNTs, which allows for assessment of conceptual and mathematical models describing coupled nanoparticle transport and deposition, and direct computation of mass balance closure, which ranged from 90.6 to 102.1% (Table 1). The amount of MWCNTs retained increased incrementally with increasing tube length (Figs. 2B and 2D). Additionally, solid-phase MWCNT concentrations decreased with increasing distance from the column inlet, a trend that is generally consistent with CBFT (Yao et al., 1971).

In order to directly observe retained MWCNTs, sand samples were collected near the column inlet and analyzed using SEM (Fig. 3). Near the column inlet, large bundles or agglomerates of MWCNTs were retained at the intersection of sand surfaces (Fig. 3A) while individual MWCNTs were deposited on sand grain surfaces (Fig. 3B). In contrast to the column inlet, individual MWCNTs were only observed deposited on surfaces (Fig. 3C), with no accumulation at grain intersections. As a reference, Fig. 3D shows a collection of sand grains at 360× magnification.

3.3. Mathematical modeling of MWCNT fate and transport

Effluent BTCs obtained for the non-reactive tracer (Br^-), plotted in Figs. 2A and 2C, were symmetrical in shape and absent of tailing. The effluent tracer data were fit to a dimensionless form of the 1-D ADR equation (CXTFIT ver. 2.1, Toride et al., 1999) to yield

an average retardation factor (R_F) of 1.01 ± 0.01 and a hydrodynamic dispersion coefficient (D_H) of 0.067 ± 0.01 cm^2/min. The fitted tracer parameters are consistent with results obtained in previous column studies conducted with the same size fraction of Ottawa sand (Wang et al., 2008b), and indicate that physical non-equilibrium processes (Weber et al., 1996), such as mass transfer into regions of immobile water, did not influence the observed MWCNT transport and retention behavior.

Initial simulations of MWCNT transport and deposition were performed using a mathematical model based on CBFT, Eqs. (1) – (3). The CBFT model accurately captured the flat plateau, as well as the sharp ascent and descent of the MWCNT BTCs (Fig. S2), yielding attachment rate coefficients that ranged from 1.9×10^{-3} to 12.7×10^{-3} min^{-1} which increased with tube length (Table S1). However, model fits to the corresponding MWCNT retention profiles were generally poor, failing to match the relatively large concentration of MWCNTs deposited near the column inlet, and the exponential decrease in retained mass with travel distance (Fig. S2). In an effort to improve the retention profile fits, the least squares fitting routine in Hydrus 1-D was modified from equal weighting of the BTC and retention profile. The weighting term for the effluent BTCs was varied from 0.001 to 2, while the retention profile weighting term was maintained at 1.0. Although the resulting solid phase concentrations of MWCNT increased in magnitude throughout the domain, the retention profiles remained relatively constant (flat) with travel distance as the value of the BTC weighting function was increased (Fig. S3). Alternatively, the attachment rate (k_{att}) was manually adjusted from 0.002 to 2.0 min^{-1} to determine if the general shape of the retention profile could be reproduced. A one order-of-magnitude increase in the value of k_{att} (i.e., from 0.002 to 0.02 min^{-1}) caused the breakthrough curve plateau to decrease from a relative concentration of 0.96 to 0.68, and greatly increased the solid phase concentrations, such that neither the simulated BTC nor the retention profile corresponded to the measured data (Fig. S4). These trends were accentuated at higher values of k_{att} (i.e., 0.4 and 2 min^{-1}), where the simulated BTCs were not observable (i.e., complete retention). The corresponding retention profile became very large although the general shape of the profile was more consistent with the elevated retention of MWCNT observed near the column inlet (Figs. S4A and S4C).

4. Discussion

4.1. MWCNT Size Distribution

MWCNTs used in this study were functionalized with 4-EBAc in phosphoric acid, which is far less aggressive than either acid treatment or ultrasonication, which are known to result in physical alteration such as reduction in tube length. Despite these efforts, the range of lengths obtained for short, medium and long classes of functionalized MWCNTs were 0.02 to 1.3μm, 0.2 to 7.5 μm, and 0.2 to 21.4 μm, and were substantially less than the corresponding values reported by the manufacturer (0.5–2 μm, 10–30 μm, and 100 μm, respectively). These findings reinforce the need to conduct careful characterization of nanotube length, rather than relying on manufacturer-reported values.

When ethoxybenzoyl moieties are covalently bonded onto the MWCNT surface, the expected increase in nanotube diameter is approximately 1 nm (Lee et al., 2008). The TEM-measured diameters of short, medium and long length classes of functionalized MWCNTs were 10–30 nm, 10–40 nm, and 30–70 nm, respectively. Comparisons of these diameters to the manufacturer-reported values for pristine MWCNTs (10–20 nm, 10–20 nm, and 8–15 nm, respectively) indicates that there was minimal association or bundling of individual nanotubes in suspensions containing short and medium tube lengths. In contrast, a greater proportion of the functionalized MWCNTs in the long size class existed in a bundled state (30–70 nm diameter), which is consistent with findings of Lee et al. (2008).

In most CNT studies conducted in aqueous suspensions, the reported hydrodynamic size is typically determined by dynamic light scattering (DLS) (e.g., Lecoanet et al., 2004; Jaisi and Elimelech, 2009). For these data, it is important to recognize that DLS size measurements are based on the diffusion of a particle in the aqueous suspension (i.e., Stokes-Einstein equation). Thus, the reported "hydrodynamic" diameter or "effective" length corresponds to the diameter of a spherical particle with the same diffusion coefficient. In this study, the effective hydrodynamic diameters determined by DLS ranged from 211–334 nm, 313–408 nm, and 600–795 nm for short, medium and long classes of MWNCTs, respectively (Table S1, Fig. S5). Both the mean value and upper range of MWCNT lengths determined by DLS were substantially less than the corresponding values obtained by TEM analysis of influent suspensions (Fig. 1, 0 PV). In addition, the DLS-determined polydispersivity index (PDI) for the MWCNT suspensions was greater than 0.4 (Table S1), indicative of particle size distributions exhibiting bi- or tri-modal shapes (Fig. S5). The findings illustrate the difficulties associated with quantifying the size characteristics of CNTs in aqueous suspension, and support the use of multiple measurement techniques (e.g., TEM and DLS) to assess relative and absolute tube lengths.

4.2. Effect of tube length on MWCNT mobility

As the tube length was increased from short to long, incremental reductions in the relative concentration plateau (from 0.97 to 0.71) were observed in column effluent BTCs for MWCNT input concentrations of both 10 and 90 mg/L (Figs. 2A and 2C, respectively). In a column study conducted with carboxyl (-COOH) functionalized SWCNTs (mean d_H ca. 120 nm by DLS), applied at an input concentration of 87 mg/L in a water-saturated sand (d_{50} = 0.26 mm) operated at a pore-water velocity of ca. 18 m/d, the relative concentration plateau only reached a value of 0.1 (Jaisi et al., 2008). In contrast, Lecoanet et al. (2004) reported nearly complete breakthrough (C/C_o = 0.95) of surfactant (sodium dodecylbenzene suflonic acid)-stabilized SWCNT in a water-saturated quartz sand (d_{50} = 0.355 mm) under similar conditions. Comparisons between these data sets indicate MWCNTs functionalized with 4-EBAc exhibit considerably greater mobility than SWCNTs stabilized by carboxyl groups, and approach the mobility of surfactant stabilized SWCNTs. Additionally, these findings highlight the dominant role that stabilizing agents and surface coatings play in CNT mobility in porous media.

In the column experiments performed with long MWCNTs at the lower input concentration (10 mg/L), and the medium and long tube lengths at the higher input concentration (90 mg/L), a concentration spike occurred near the end of the plateau period, corresponding to the completion of the MWCNT pulse injection and introduction of the MWCNT-free background electrolyte solution (Figs. 2A and 2C). Here, we hypothesize that the brief period of flow stoppage (< 30 sec) followed by the re-initiation of flow caused MWCNTs that were loosely attached on sand surface, to be dislodged and subsequently transported through the column. This hypothesis is consistent with the increase in effluent MWCNT concentrations observed in the first pore volume of effluent solution collected after flow recommenced (i.e., 4–5 PVs, Figs. 2A and 2C), where the highest concentrations correspond to displaced resident solution closest to column inlet (i.e., later time). Although the background electrolyte solutions were adjusted to have the same ionic strength as the MWCNT suspensions (6 or 75 mM), differences in the electrolyte composition (i.e., presence of residual phosphate in the suspension) may have contributed to the observed release of MWCNTs following the pulse injection.

4.3. Effect of tube length on MWCNT retention

The MWCNT retention profiles exhibited elevated deposition near the column inlet, which increased with increasing tube length and was accentuated at the higher input concentration

(Figs. 2B and 2D). The hyper-exponential shape of the retention profiles obtained for MWCNTs is distinct from those observed for C_{60} fullerene nanoparticles under similar conditions, which exhibited relatively constant retention that could be described mathematically using a maximum or limiting retention capacity blocking function (Li et al., 2008;Wang et al., 2008b). These MWCNT retention profiles are among the first to be reported and demonstrate the potential importance of variable deposition with travel distance, which may be indicative of physical straining.

In order to further evaluate the effect of tube length on MWCNT transport, and, more specifically, preferential retention of longer tuber lengths, five effluent samples from each of the higher input concentration experiments (90 mg/L) were imaged using TEM (Fig. 1). Effluent samples were selected to correspond to the ascending (ca. 1.1 PV), plateau (ca. 2.3, 3.6, and 4.7 PVs), and descending portions of the BTCs (ca. 6.0 PVs). In addition, TEM specimens were prepared from samples collected directly from syringe prior to injection (0 PV). For short (0.02 to 1.3 μm) MWCNTs, greater than 80% of total counted tubes exhibited lengths of less than 0.5 μm, although lengths greater than 1 μm were present in all samples except at 1.1 PV. The medium MWCNT (0.2 to 7.5 μm) input suspension contained a small number of tubes with lengths greater than 7 μm, which were not observed in any of the effluent samples. A similar trend was observed with the longest size fraction of MWCNTs (0.2 to 21.4 μm), where tubes lengths of greater than 11 μm were not detected in any of the effluent samples. These findings suggest that MWCNTs with length greater than approximately 8 μm were preferentially retained in 40–50 quartz sand, while retention was not selective for tube lengths of less than 8 μm. The narrower length distribution of effluent MWCNTs compared to the influent suspension suggests that physical straining may have contributed to MWCNT retention (Bradford et al., 2006).

4.4. Mechanisms governing MWCNT transport and deposition

Although the mathematical model based on CBFT was able to accurately represent the observed MWNT effluent BTC data (Figs. S2A and S2B), the model was unable to simulate the observed retention profiles (Figs. S2C and S2D). Despite efforts to improve the CBFT model predictions of measured retention data, either by increasing the weight given to the retention data in the fitting routine (Fig. S3), or by manually adjusting the attachment rate parameter (Fig. S4), the CBFT model was not able to capture the shape of the MWCNT retention profiles. The discrepancy between the measured and fitted retention profiles was primarily due to large solid-phase concentrations detected near the column inlet, which was most apparent for MWCNTs with the longest tube lengths (0.2 to 21.4 μm). This type of retention profile could result from physicochemical deposition subject to a heterogeneous attachment rate coefficient among the particle population. For example, Tufenkji et al. (2003) successfully simulated a hyper-exponential retention profile of bacteria in glass beads by coupling a power law distribution of k_{att} into CBFT. Following a similar approach, the CBFT model was modified to incorporate a k_{att} power law distribution function, the overall fit to MWCNT retention profiles improved (Fig. S6) compared to the unmodified CBFT model fits. However, the model still lacked the ability to capture the MWCNT solid phase concentration near column inlet under these experimental conditions.

The hyper-exponential-decaying retention profiles could be a result of sand surface heterogeneity because particle-sand interactions are strongly dependent upon the local surface charge, shape, and roughness (Li et al., 2006). As shown in Fig. 3, the surface of quartz sand under current experimental conditions was heterogeneous at both micron and millimeter scales. However, arguments against this hypothesis include that the parallel (to surface) deposition of individual nanotubes on both rough and smooth regions of the sand surfaces. Therefore, surface heterogeneity was not considered to be a dominant factor contributing to elevated MWCNT retention near the column inlet.

Alternatively, the shape of retention profile could be indicative of a system that is subject to physical straining, where particles are retained or trapped at intersections of grain-to-grain contact points, which ultimately may result in pore throat blockage. For example, Bradford et al. (2003) reported almost complete retention of 2 μm latex microspheres at the inlet of columns packed with either quartz sand or glass beads. Based on comparisons with fullerene (C_{60}) retention and responses to changes in solution chemistry, Jaisi and Elimelech (2009) concluded that physical straining controlled the filtration and transport of carboxyl-functionalized SWCNTs (0.6 to 8 μm tube length) in a water-saturated soil (aggregate sizes of 0.42 to 1.00 mm). Therefore, a physical straining expression presented in Eqs. (4) and (5), was incorporated into the mathematical model. This modification greatly improved model fits to the MWCNT retention profile data (Fig. 2), with minimal impact on the BTC fits relative to those obtained when the unmodified or power law distribution CBFT model. The resulting physical straining rates (k_{str}) were more than four orders-of-magnitude greater than the corresponding attachment rates (k_{att}), which ranged from 8.29×10^{-8} to 9.15×10^{-5} min^{-1} (Table 1). These findings suggest that the physical straining contributed far more significantly to MWCNT retention than traditional physico-chemical deposition processes under the conditions investigated herein, consistent with the findings of (Jaisi and Elimelech, 2009) for SWCNTs in an aggregated soil. Furthermore, the fitted straining rates increased substantially with increasing tube length; where the straining rates obtained for long MWCNTs were two orders-of-magnitude greater than those of the short MWCNTs. Although physical straining appears to have played a dominant role in MWCNT retention near the column inlet, it should be also noted that more than 75% of total delivered MWCNT mass was transported through the column (Table 1). This rather high mobility is attributed to the relatively large negative surface charge of the functionalized MWCNTs (ca. −40 mV), coupled with the potential alignment of the shorter nanotubes with the local flow direction, a phenomenon that has been observed with non-spherical latex microspheres (Xu et al. 2008).

5. Conclusions

This study provides new information on the transport and retention behavior of MWCNTs in water-saturated quartz sand. The results of this work are relevant to the assessment and prediction of MWCNT fate and transport in subsurface environments, and the performance of drinking water filtration systems. Although extrapolation of these findings to field sites and engineered systems should be done with caution, the major conclusions of this study include:

- Functionalization of MWCNT with 4-ethoxybenzoic acid (4-EBAc) yielded stable suspensions that were readily transported through a water-saturated quartz sand with greater than 76% of the applied mass detected in the column effluent under all experimental conditions.
- A mathematical model based on Clean bed filtration theory (CBFT) was able to accurately capture MWCNT effluent breakthrough curves (BTCs), but could not adequately simulate the observed retention behavior despite varying the weighting function and incorporating a nonuniform attachment rate coefficient.
- Incorporation of a particle straining term in CBFT model allowed for accurate predictions of both MWCNT effluent BTCs and retention profiles, and yielded particle straining rates that were four orders-of-magnitude greater than the previously obtained attachment rates.
- A combination of experimental measurements (hyperexponential retention profiles and preferential retention of longer tube lengths), direct observation (SEM images of MWCNT agglomerates at grain intersections) and mathematical model

simulations (greatly improved fits to effluent BTCs and retention profiles), indicate that physical straining played an important role in the retention of MWCNTs for the experimental conditions considered herein.

Supplementary Material

Refer to Web version on PubMed Central for supplementary material.

Acknowledgments

We thank Dr. Howard Fairbrother at Johns Hopkins University for his helpful suggestions and Dr. Yusong Li at University of Nebraska and Dr. Li Wang at Tetra Tech Inc. for their assistance on Hydrus-1D. Support for this research was provided by grants from the National Science Foundation (CBET-0854136), the National Institute of Environmental Health, National Institutes of Health (R01-ES016175) and World Class University (WCU).

References

Bradford SA, Šimůnek J, Bettahar M, Van Genuchten MT, Yates SR. Modeling colloid attachment, straining, and exclusion in saturated porous media. Environmental Science & Technology. 2003; 37:2242–2250. [PubMed: 12785531]

Bradford SA, Simunek J, Bettahar M, van Genuchten MT, Yates SR. Significance of straining in colloid deposition: Evidence and implications. Water Resources Research. 2006; 42:W12S15.

Cui DX, Tian FR, Ozkan CS, Wang M, Gao HJ. Effect of single wall carbon nanotubes on human HEK293 cells. Toxicology Letters. 2005; 155:73–85. [PubMed: 15585362]

Davoren M, Herzog E, Casey A, Cottineau B, Chambers G, Byrne HJ, Lyng FM. In vitro toxicity evaluation of single walled carbon nanotubes on human A549 lung cells. Toxicology in Vitro. 2007; 21:438–448. [PubMed: 17125965]

Gannon CJ, Cherukuri P, Yakobson BI, Cognet L, Kanzius JS, Kittrell C, Weisman RB, Pasquali M, Schmidt HK, Smalley RE, Curley SA. Carbon nanotube-enhanced thermal destruction of cancer cells in a noninvasive radiofrequency field. Cancer. 2007; 110:2654–2665. [PubMed: 17960610]

Hiemenz, PC.; Rajagopalan, R. Principles of Colloid and Surface Chemistry. 3rd ed. Marcel Dekker, Inc.; New York: 1997.

Hussain MA, Kabir MA, Sood AK. On the cytotoxicity of carbon nanotubes. Current Science. 2009; 96:664–673.

Hyung H, Fortner JD, Hughes JB, Kim JH. Natural organic matter stabilizes carbon nanotubes in the aqueous phase. Environmental Science & Technology. 2007; 41:179–184. [PubMed: 17265945]

Jaisi DP, Saleh NB, Blake RE, Elimelech M. Transport of single-walled carbon nanotubes in porous media: filtration mechanisms and reversibility. Environmental Science & Technology. 2008; 42:8317–8323. [PubMed: 19068812]

Jaisi DP, Elimelech M. Single-walled carbon nanotubes exhibit limited transport in soil columns. Environmental Science & Technology. 2009; 43:9161–9166. [PubMed: 20000506]

Jiang JK, Oberdorster G, Biswas P. Characterization of size, surface charge, and agglomeration state of nanoparticle dispersions for toxicological studies. Journal of Nanoparticle Research. 2009; 11:77–89.

Kong J, Franklin NR, Zhou CW, Chapline MG, Peng S, Cho KJ, Dai HJ. Nanotube molecular wires as chemical sensors. Science. 2000; 287:622–625. [PubMed: 10649989]

Lecoanet HF, Bottero JY, Wiesner MR. Laboratory assessment of the mobility of nanomaterials in porous media. Environmental Science & Technology. 2004; 38:5164–5169. [PubMed: 15506213]

Lecoanet HF, Wiesner MR. Velocity effects on fullerene and oxide nanoparticle deposition in porous media. Environmental Science & Technology. 2004; 38:4377–4382. [PubMed: 15382867]

Lee HJ, Han SW, Kwon YD, Tan LS, Baek JB. Functionalization of multi-walled carbon nanotubes with various 4-substituted benzoic acids in mild polyphosphoric acid/phosphorous pentoxide. Carbon. 2008; 46:1850–1859.

Li Y, Wang Y, Pennell KD, Abriola LM. Investigation of the transport and deposition of fullerene (C60) nanoparticles in quartz sand under varying flow conditions. Environmental Science & Technology. 2008; 42:7174–7180. [PubMed: 18939543]

Li C, Chen YH, Wang YB, Iqbal Z, Chhowalla M, Mitra S. A fullerene-single wall carbon nanotube complex for polymer bulk heterojunction photovoltaic cells. Journal of Materials Chemistry. 2007; 17:2406–2411.

Li XQ, Lin C, Miller JD, Johnson WP. Role of grain-to-grain contacts on profiles of retained colloids in porous media in the presence of an energy barrier to deposition. Environmental Science & Technology. 2006; 40:3769–3774. [PubMed: 16830540]

Liu XY, O'Carroll DM, Petersen EJ, Huang QG, Anderson CL. Mobility of multiwalled carbon nanotubes in porous media. Environmental Science & Technology. 2009; 43:8153–8158. [PubMed: 19924937]

Rasband, WS. ImageJ. U.S. National Institutes of Health; Bethesda, Maryland, USA: 2011. http://imageJ.nih.gov/ij

Šimůnek, J.; Šejna, M.; Saito, H.; Sakai, M.; van Genuchten, M. Th. The Hydrus-1D Software Package for Simulating the Movement of Water, Heat, and Multiple Solutes in Variably Saturated Media. Version 4.0. Department of Environmental Sciences, University of California Riverside; Riverside, CA: 2008. HYDRUS Software Series 3

Sun YP, Fu KF, Lin Y, Huang WJ. Functionalized carbon nanotubes: Properties and applications. Accounts of Chemical Research. 2002; 35:1096–1104. [PubMed: 12484798]

Toride, N.; Leij, FJ.; vanGenuchten, MT. The CXTFIT code for estimating transport parameters from laboratory or field tracer experiments. Version 2.1. Riverside, CA: 1999. Research report No. 137

Tufenkji N, Redman JA, Elimelech M. Interpreting deposition patterns of microbial particles in laboratory-scale column experiments. Environmental Science & Technology. 2003; 37:616–623. [PubMed: 12630480]

Wang P, Shi QH, Liang HJ, Steuerman DW, Stucky GD, Keller AA. Enhanced environmental mobility of carbon nanotubes in the presence of humic acid and their removal from aqueous solution. Small. 2008a; 4:2166–2170. [PubMed: 19058159]

Wang YG, Li YS, Fortner JD, Hughes JB, Abriola LM, Pennell KD. Transport and retention of nanoscale C-60 aggregates in water-saturated porous media. Environmental Science & Technology. 2008b; 42:3588–3594. [PubMed: 18546694]

Wang XS, Li QQ, Xie J, Jin Z, Wang JY, Li Y, Jiang KL, Fan SS. Fabrication of ultralong and electrically uniform single-walled carbon nanotubes on clean substrates. Nano Letters. 2009; 9:3137–3141. [PubMed: 19650638]

Weber, WJ.; Pennell, KD.; Dekker, TJ.; Abriola, LM. Sorption and retardation of organic contaminants in subsurface systems: Effect on transport and fate. In: Aral, MM., editor. Advances in groundwater pollution control and remediation. Kluwer Academic; The Netherlands: 1996. p. 1-31.

Xu SP, Liao Q, Saiers JE. Straining of nonspherical colloids in saturated porous media. Environmental Science & Technology. 2008; 42:771–778. [PubMed: 18323101]

Yao KM, Habibian MM, Omelia CR. Water and waste water filtration - concepts and applications. Environmental Science & Technology. 1971; 5:1105–1112.

Highlights

- Functionalized MWCNT were readily transported through water-saturated quartz sand.
- MWCNT retention was elevated near the column inlet and longer tubes were preferentially retained.
- Scanning electron microscope (SEM) images provide direct evidence of physical straining.
- A clean bed filtration theory (CBFT) model was unable to simulate MWCNT retention profiles.
- Incorporation of a particle straining term greatly improved model predictions.

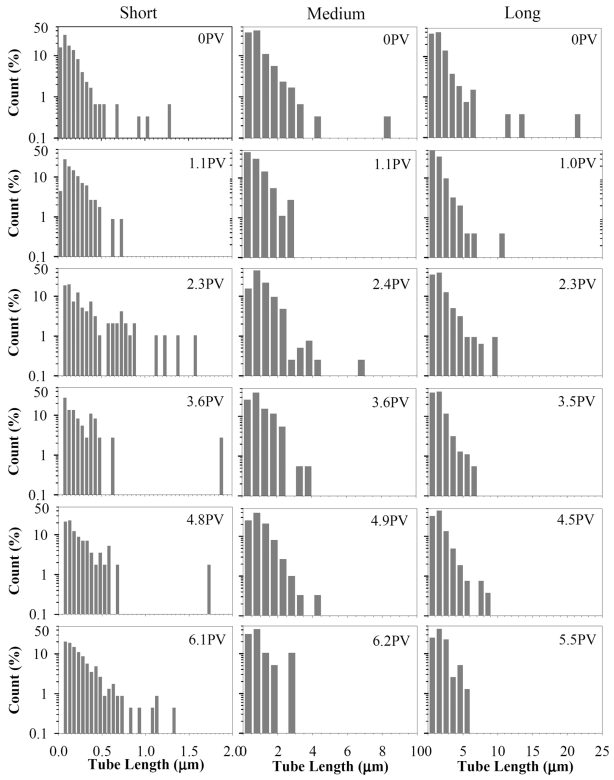

Fig. 1.

Length histogram of MWCNTs obtained from TEM image analysis of samples collected immediately prior to injection (0 PV) and in column effluent samples. Each bar represents a length range of 0.05, 0.5, and 1 μm for short-, medium-, and long-MWCNTs, respectively.

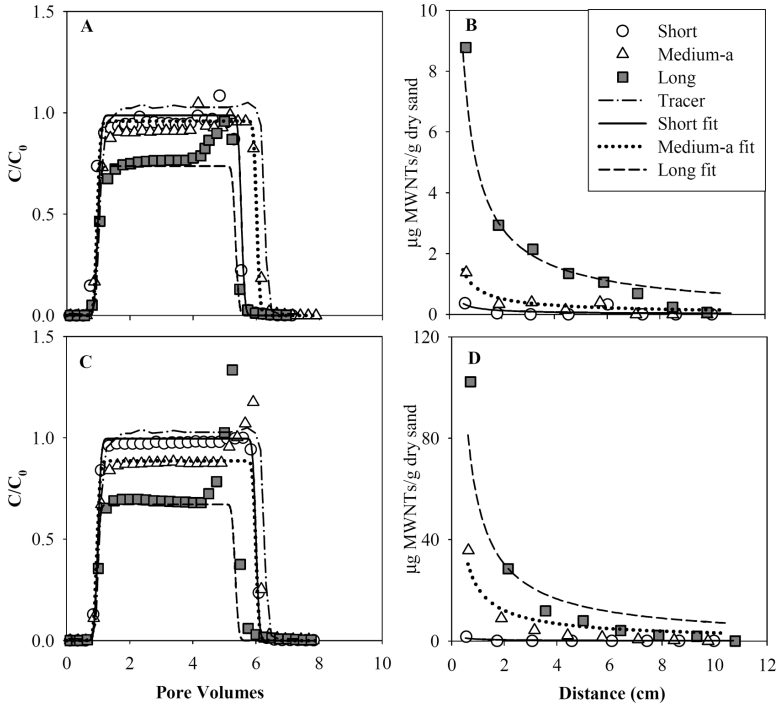

Fig. 2.

Comparisons of measured and fitted effluent breakthrough curves and retention profiles of short, medium, and long MWCNTs applied to water-saturated columns packed with 40–50 mesh Ottawa sand at input concentrations of 10 mg/L (A and B) or 90 mg/L (C and D). Experimental data were fit to a modified CBFT model that accounted for first order attachment and physical straining.

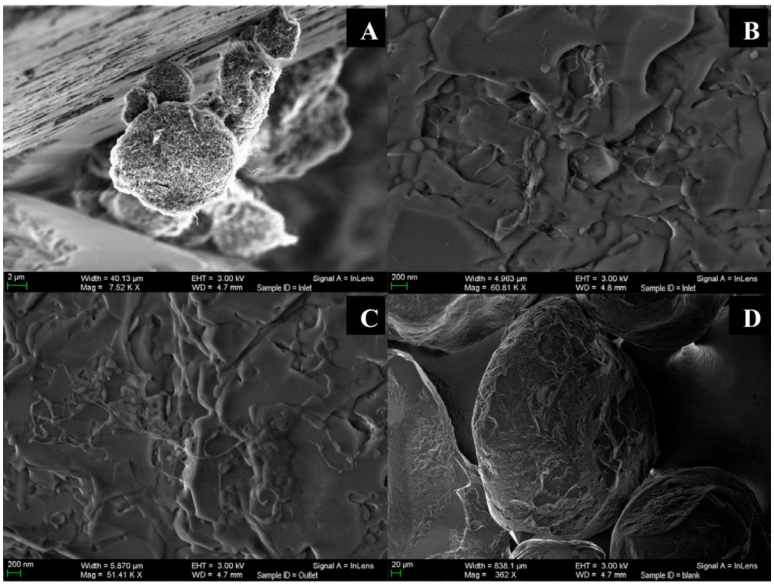

Fig. 3.

Representative scanning electron microscopy (SEM) images of retained MWCNTs near the column inlet (A and B), column outlet (C), and of the porous media at lower magnification (D). Samples were collected following a 3PV injection of aqueous suspension containing medium MWCNT (0.2–7.5 μm) with an input concentration of 90 mg/L. The scale bars for panels (A), (B), (C), and (D) correspond to 2 μm, 200 nm, 200 nm, and 20 μm, respectively.

Table 1

Experimental conditions and simulation parameters for transport and retention of with three size fractions of MWCNTs conducted in 1-D columns packed with 40–50 mesh (d_{50} = 0.36 mm) quartz sand and operated at a pore-water velocity of 7.6 m/day.

Column Identifier[a]	PW[b] PV	IS[c] mM	EM[d] μm·cm/V·s	Ret[e] %	MB[f] %	$K_{att}\times10^{-7}\ min^{-1}$	95%CL[g] $\times10^{-4}$	$K_{str}\times10^{-2}\ min^{-1}$	95%CL $\times10^{-2}$	MMB[h] %
Short-10	4.5	6	−3.0±0.1	1.0	90.6	0.83	±4.86	1.76	±1.17	99.9
Medium-10a	5.1	6	−3.4±0.1	2.9	95.6	4.66	±5.07	5.57	±1.28	99.9
Medium-10b	5.0	6	−3.3±0.1	3.0	93.9	6.69	±4.00	5.03	±0.95	99.8
Long-10	4.4	6	−3.8±0.0	20.3	99.3	10.9	±37.4	41.40	±9.80	99.3
Short-90	5.0	75	−2.6±0.1	0.2	98.7	1.26	±0.85	0.51	±0.72	99.8
Medium-90a	5.0	75	−3.0±0.2	6.7	98.9	5.37	±16.7	16.3	±4.22	99.8
Medium-90b	6.3	75	−3.1±0.0	6.7	98.7	915	±12.8	16.0	±3.20	99.5
Long-90	4.4	75	−3.2±0.1	23.7	102.1	4.48	±53.6	53.6	±15.6	95.4

[a] Short, medium and long designation corresponds to MWCNTs with measured length ranges of 0.02–1.3, 0.2– 7.5, and 0.2–21.4 μm, 10 and 90 designation indicates the input concentration, and *a* and *b* represent replicate columns.

[b] pulse width.

[c] ionic strength.

[d] electrophoretic mobility.

[e] retention.

[f] overall mass balance, equal to the sum of curve areas underneath BTC and retention profile divided by total input mass.

[g] 95% confidence limit. The confidence limit pertained to the fitted value for k_{att} or k_{str}, and was generated during the parameter optimization using a Levenberg-Marquardt algorithm. The high confidence limit relative to fitted value indicates that the optimization function is not sensitive to the fitting parameter (Simunek et al., 2008)

[h] overall mass balance in modeling